Inorg. Chem. **2005**, *44*, 8988–8998

Examination of the Bonding in Binary Transition-Metal Monophosphides MP (M = Cr, Mn, Fe, Co) by X-Ray Photoelectron Spectroscopy

Andrew P. Grosvenor,* Stephen D. Wik, Ronald G. Cavell, and Arthur Mar

Department of Chemistry, University of Alberta, Edmonton, Alberta, Canada T6G 2G2

Received June 20, 2005

The binary transition-metal monophosphides CrP, MnP, FeP, and CoP have been studied with X-ray photoelectron spectroscopy. The shifts in phosphorus $2p_{3/2}$ core line binding energies relative to that of elemental phosphorus indicated that the degree of ionicity of the metal–phosphorus bond decreases on progressing from CrP to CoP. The metal $2p_{3/2}$ core line binding energies differ only slightly and show similar line shapes to those of the elemental metals, reaffirming the notion that these transition-metal phosphides have considerable metallic character. The satellite structure observed in the Co $2p_{3/2}$ X-ray photoelectron spectra of Co metal and CoP was examined by reflection electron energy loss spectroscopy and has been attributed to plasmon loss, not final state effects as has been previously suggested. Valence-band spectra of the transition-metal phosphides agree well with the density of states profiles determined from band structure calculations. The electron populations of the different electronic states were extracted from the fitted valence-band spectra, and these confirm the presence of strong M–P and weak P–P bonding interactions. Atomic charges determined from the P 2p core line spectra and the fitted valence-band spectra support the approximate formulation $M^{1+}P^{1-}$ for these phosphides.

1. Introduction

The first-row transition metals form a series of monophosphides, MP (M = Sc−Ni), whose structures and properties have been extensively investigated. There is a progression of structure types, from NaCl-type (ScP) to TiAs-type (TiP), NiAs-type (VP), MnP-type (CrP, MnP, FeP, CoP), and NiP-type (NiP), in which successive distortions arise from the interplay of metal−metal and phosphorus−phosphorus bonding.[1] These compounds exhibit a wealth of interesting physical properties; they are all metallic, and many display unusual magnetic ordering transitions.[2] For example, a large body of work is available on MnP alone, which undergoes transitions to ferromagnetic and helimagnetic phases.[3,4] Study of the size-dependent properties of MnP and FeP nanoparticles has now begun.[5,6] CoP and other transition-metal phosphides may have applications as hydrodesulfurization and hydrodenitrogenation catalysts.[7]

To analyze the bonding in these monophosphides in more detail, it is desirable to focus on a series of isostructural members. Here we select the four MnP-type members: CrP, MnP, FeP, and CoP.[8,9] This structure, shown in Figure 1, is based on a distortion of the NiAs-type, one of the most celebrated structure types in intermetallic chemistry.[10] The metal atoms occupy all the octahedral sites between hcp layers of phosphorus atoms, so that columns of face-sharing metal-centered octahedra develop along the stacking axis. To a first approximation, the electronic structure of these compounds consists of bands that arise from the interaction of metal 3d, 4s, and 4p orbitals with the phosphorus 3s and 3p orbitals. The result is a filled, lower-energy, set of M−P bonding levels, a partially filled set of mostly metal-based d levels (split into t_{2g} and e_g components), and an empty, higher-energy, set of M−P antibonding levels.[11−13] In the

* To whom correspondence should be addressed. E-mail: andrew.grosvenor@ualberta.ca.

(1) Aronsson, B.; Lundström, T.; Rundqvist, S. *Borides, Silicides and Phosphides*; Methuen: London, 1965.
(2) Hulliger, F. *Struct. Bonding* **1968**, *4*, 83−229.
(3) Huber, E. E., Jr.; Ridgley, D. H. *Phys. Rev. Sect. A* **1964**, *135*, 1033−1040.
(4) Okabayashi, J.; Tanaka, K.; Hashimoto, M.; Fujimori, A.; Ono, K.; Okusawa, M.; Komatsubara, T. *Phys. Rev. B: Condens. Matter Mater. Phys.* **2004**, *69*, 132411-1−132411-4.
(5) Perera, S. C.; Tsoi, G.; Wenger, L. E.; Brock, S. L. *J. Am. Chem. Soc.* **2003**, *125*, 13960−13961.
(6) Perera, S. C.; Fodor, P. S.; Tsoi, G. M.; Wenger, L. E.; Brock, S. L. *Chem. Mater.* **2003**, *15*, 4034−4038.
(7) Oyama, S. T. *J. Catal.* **2003**, *216*, 343−352.
(8) Rundqvist, S. *Acta Chem. Scand.* **1962**, *16*, 287−292.
(9) Rundqvist, S.; Nawapong, P. C. *Acta Chem. Scand.* **1965**, *19*, 1006−1008.
(10) Pearson, W. B. *The Crystal Chemistry and Physics of Metals and Alloys*; Wiley-Interscience: New York, 1972.

10.1021/ic051004d CCC: $30.25
Published on Web 10/22/2005

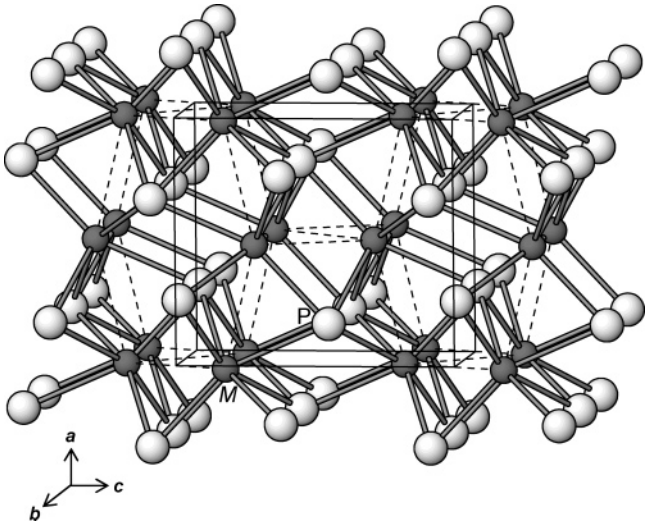

Figure 1. MnP-type crystal structure of MP (M = Cr, Mn, Fe, Co) viewed down the *b* axis. The small solid spheres are M atoms and the large lightly shaded spheres are P atoms. The dashed lines indicate the metal−metal bonding network (2.6−2.8 Å).

orthorhombic MnP-type structure, there is metal−metal bonding not only along the columns of face-sharing octahedra along the *a* direction but also between the columns in the form of zigzag chains running along the *b* direction. The metal−metal bonding network originates from the interaction between the metal-based t_{2g} orbitals, whose lobes are directed away from the metal−phosphorus bonds. These metal−metal interactions are quite strong, as indicated by bond lengths of 2.6−2.8 Å.[9] The t_{2g}-based bands are expected to broaden and overlap significantly with the e_g-based bands with no gap between them. The structural distortion also generates zigzag chains of phosphorus atoms running along the *b* direction but at distances (2.6−2.7 Å)[9] that are somewhat longer than the typical single P−P covalent bond length of 2.2 Å.[14] Several questions arise. To what extent does electron transfer occur from metal to phosphorus atoms? How reasonable are formulations such as $M^{3+}P^{3-}$ (which assumes isolated P anions) or $M^{1+}P^{1-}$ (which assumes 2 center-2e$^-$ bonds in the zigzag chains of P atoms)? How closely does the metal−metal bonding character in these compounds resemble that in the elemental metals?

The electronic structure of some first-row transition-metal monophosphides has been previously investigated with both experimental X-ray photoelectron spectroscopy (XPS) studies[15−18] and theoretical calculations.[11−13,19,20] Here we describe new high-resolution XPS measurements of CrP, MnP, FeP, and CoP, with the goal of clarifying the electronic structure and bonding in these important compounds. In particular, the metal 2p and phosphorus 2p binding energies have been measured, and the trends in these energies have been related to the degree of covalency in the metal-phosphorus bonds. For the first time, the metal $2p_{3/2}$ peak shapes in these monophosphides have been analyzed in detail and compared to those in clean samples of the parent transition metal. The origin of the satellite structure found in the Co $2p_{3/2}$ spectra in Co metal and in CoP will also be discussed. Valence orbital electron populations in these compounds were extracted, for the purpose of bonding analyses, from peak fitting deconvolution of the valence-band spectra.

2. Experimental Section

2.1. Synthesis. The monophosphides were prepared from stoichiometric reaction of Cr (99.95%, Alfa-Aesar), Mn (99.95%, Cerac), Fe (99.9%, Cerac), or Co (99.999%, Spex) metal powder with red P (99.995%, Cerac), placed in evacuated fused-silica tubes. The tubes were heated to 1323 K over a 36-h period and maintained at this temperature for 4 days before being cooled over 12 h to room temperature. The products were isolated and stored in a glovebox under argon to limit exposure to air. The powder X-ray diffraction patterns, obtained on an Inel powder diffractometer equipped with a CPS 120 detector, were in good agreement with those calculated from the literature crystallographic data and revealed that the samples represented pure phases.

2.2. XPS Analysis. All measurements were performed on a Kratos AXIS Ultra spectrometer equipped with a monochromatic Al Kα X-ray source. The pressures throughout the analysis chamber were 10^{-6}−10^{-7} Pa. The resolution function for this instrument has been determined to be 0.4 eV by analysis of the cobalt Fermi edge.

Samples were finely ground in a glovebox and pressed into 0.5-mm thick In foil (Alfa-Aesar) before being placed on a Cu sample holder and transferred to the XPS instrument in a sealed container to reduce exposure to air during transport. After being loaded into the instrument, the samples were sputter-cleaned with an Ar^+ ion beam (4 kV, 10 mA) to remove any surface oxide or phosphate which had formed. The time required for sputter-cleaning depended on the degree of oxidation present (as ascertained by initial survey spectra of the as-received samples) and ranged from 10 (CoP) to 45 min (MnP). After the samples were sufficiently clean, both survey (broad range) and high-resolution spectra were obtained. Survey spectra were collected with a binding energy (BE) range of 0−1100 eV, a pass energy of 160 eV, a step size of 0.7 eV, a sweep time of 180 s, and a spot size of 700 × 400 μm^2. High-resolution spectra were collected with an energy envelope of 20−45 eV (depending on the peak being examined (phosphorus 2p, metal $2p_{3/2}$, or valence band)), a pass energy of 20 eV, and a step size of 0.05 eV. All results were analyzed with use of the CasaXPS software package.[21] During this study, it was found that charge correction was not required, most likely because of the metallic

(11) Yanase, A.; Hasegawa, A. *J. Phys. C: Solid State Phys.* **1980**, *13*, 1989−1993.
(12) Perkins, P. G.; Marwaha, A. K.; Stewart, J. J. P. *Theor. Chim. Acta* **1981**, *59*, 569−583.
(13) Tremel, W.; Hoffmann, R.; Silvestre, J. *J. Am. Chem. Soc.* **1986**, *108*, 5174−5187.
(14) Pauling, L. *The Nature of the Chemical Bond*, 3rd ed.; Cornell University Press: Ithaca, NY, 1960.
(15) Domashevskaya, E. P.; Terekhov, V. A.; Ugai, Ya. A.; Nefedov, V. I.; Sergushin, N. P.; Firsov, M. N. *J. Electron Spectrosc. Relat. Phenom.* **1979**, *16*, 441−453.
(16) Myers, C. E.; Franzen, H. F.; Anderegg, J. W. *Inorg. Chem.* **1985**, *24*, 1822−1824.
(17) Okuda, H.; Senba, S.; Sato, H.; Shimada, K.; Namatame, H.; Taniguchi, M. *J. Electron Spectrosc. Relat. Phenom.* **1999**, *101*−*103*, 657−660.
(18) Shabanova, I. N.; Mitrochin, Y. S.; Terebova, N. S.; Nebogatikov, N. M. *Surf. Interface Anal.* **2002**, *34*, 606−609.
(19) Noläng, B.; Eriksson, O.; Johansson, B. *J. Phys. Chem. Solids* **1990**, *51*, 1033−1046.
(20) Scott, B. A.; Eulenberger, G. R.; Bernheim, R. A. *J. Chem. Phys.* **1968**, *48*, 263−272.
(21) Fairley, N. *CasaXPS*, version 2.2.19; Casa Software Ltd.: Teighnmouth, Devon, UK, 2003 (www.casaxps.com).

nature of these compounds. To fit the high-resolution spectra, a Shirley-type function was first used to remove the background arising from energy loss. The extracted spectra were then fitted with a combined Gaussian (70%) and Lorentzian (30%) line profile to account for spectrometer and lifetime broadening, respectively. The chemical compositions of the samples were determined from both these X-ray photoelectron (XP) survey spectra and independent EDX analysis (Hitachi S-2700 SEM; 20 kV beam voltage). Within experimental accuracy, all samples were essentially stoichiometric (50 ± 5% M; 50 ± 5% P).

XP spectra of metal standards were also collected. Samples (in the form of foils or pieces) of Cr (Fisher Scientific), Mn (99.98%, Alfa-Aesar), Fe (99.995%, Alfa-Aesar), and Co (99.0%, British Drug House) metal were sputter-cleaned to remove any surface oxide present and analyzed using similar parameters as above. Both survey and high-resolution spectra (metal $2p_{3/2}$ and valence band) were obtained.

2.3. REELS Analysis. To examine the nature of the satellite peaks observed in the XP spectrum of Co metal (99.995%, Alfa-Aesar), reflection electron energy loss spectroscopy (REELS) was performed on a PHI 660 scanning Auger microprobe with electron beam energies of 3−0.2 keV. Before analysis, the sample was cleaned in situ by Ar^+ ion-beam sputtering at 3 kV. The sample was considered suitably clean when no O KLL line was observed in the Auger spectra. This analysis was performed at Surface Science Western (SSW) at the University of Western Ontario (UWO).

2.4. Band Structure Calculations. Although theoretical calculations have been previously performed on some MnP-type compounds, it was desirable to extract partial density of states profiles for the metal and phosphorus valence states to illustrate the fitting of the experimental valence-band spectra here. A tight-binding extended Hückel band structure calculation on MnP was performed with 96 *k*-points in the irreducible portion of the Brillouin zone, with use of the EHMACC suite of programs,[22,23] The atomic parameters (valence shell ionization potentials H_{ii} (eV) and orbital exponents ζ_i) were as follows. For Mn 4s, $H_{ii} = -9.8$, $\zeta_i = 1.80$; for Mn 4p, $H_{ii} = -5.9$, $\zeta_i = 1.80$; for Mn 3d, $H_{ii} = -11.7$, $\zeta_{i1} = 5.15$, $c_1 = 0.514$, $\zeta_{i2} = 1.70$, $c_2 = 0.693$; for P 3s, $H_{ii} = -18.6$, $\zeta_i = 1.84$; for P 3p, $H_{ii} = -14.0$, $\zeta_i = 1.45$.

3. Results and Discussion

3.1. Phosphorus 2p High-Resolution X-Ray Photoelectron Spectra. Figure 2 shows the high-resolution phosphorus 2p XP spectra collected for CrP, MnP, FeP, and CoP. Each spectrum shows two peaks corresponding to the P $2p_{3/2}$ (low binding energy) and P $2p_{1/2}$ (high binding energy) states. Sharp line shapes were observed which could be fitted with component peaks having a FWHM as small as 0.7 eV. In all cases, the intensity ratio of the P $2p_{3/2}$ and $2p_{1/2}$ peaks was 2:1, which is consistent with the expected ratio of $(2j_1 + 1)/(2j_2 + 1)$, where j_1 and j_2 represent the coupled orbital (l) and spin (s) angular momentum quantum numbers from respective spin-up and spin-down states of the unpaired core electron which remains after photoionization.[24] On progressing through the series CrP to CoP, the P $2p_{3/2}$ and $2p_{1/2}$ binding energies gradually increase (Table 1). On the high-binding-energy side in all spectra, there is a small peak which is attributed to the P $2p_{1/2}$ signal from some remaining unreacted phosphorus; the corresponding P $2p_{3/2}$ peak is not indicated, as it would be buried under the main P $2p_{1/2}$ peak from the transition-metal monophosphide.

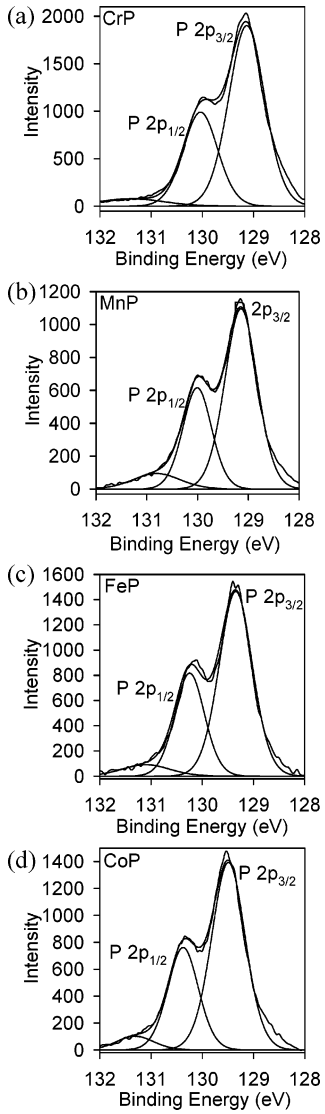

Figure 2. High-resolution P 2p XP spectra of (a) CrP, (b) MnP, (c) FeP, and (d) CoP. Here and in other spectra, the intensity is in counts per second (cps).

Table 1. Binding Energies (eV) of Core Photoelectron Peaks in Transition-Metal Monophosphides MP (M = Cr, Mn, Fe, Co) and Metal Standards

	CrP	MnP	FeP	CoP
P $2p_{1/2}$	130.0	130.2	130.2	130.4
P $2p_{3/2}$	129.1	129.2	129.3	129.5
M $2p_{3/2}$	573.9	638.7	706.9	778.3 (781.4, 783.0)[a]
	Cr	**Mn**	**Fe**	**Co**
M $2p_{3/2}$	574.1	638.7	707.0	778.1 (781.1, 783.1)[a]

[a] Satellite peaks arising from plasmon loss processes.

(22) Whangbo, M.-H.; Hoffmann, R. *J. Am. Chem. Soc.* **1978**, *100*, 6093−6098.
(23) Hoffmann, R. *Solids and Surfaces: A Chemist's View of Bonding in Extended Structures*; VCH Publishers: New York, 1988.
(24) Briggs, D., Seah, M. P., Eds. *Practical Surface Analysis, Vol. 1: Auger and X-ray Photoelectron* Spectroscopy, 2nd ed.; Wiley: Chichester, 1990.

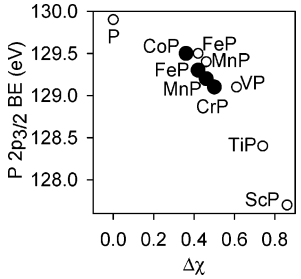

Figure 3. Plot of P $2p_{3/2}$ binding energies, BE, versus the difference in electronegativity (Allred−Rochow) between the phosphorus and metal atoms, $\Delta\chi$,[25] for several first-row transition-metal monophosphides. Values indicated by solid circles (●) are from this work, and those by open circles (○) are from ref 16.

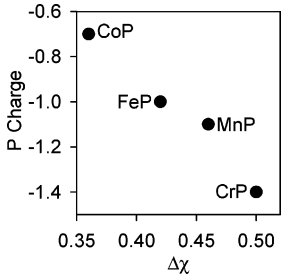

Figure 4. Plot of the charge on P atoms (estimated from binding energy values) versus the difference in electronegativity, $\Delta\chi$, for CrP, MnP, FeP, and CoP.

Figure 3 shows a plot of the P $2p_{3/2}$ binding energies versus the difference in electronegativity (Allred−Rochow)[25] between the phosphorus and metal atoms for these and other first-row transition-metal monophosphides. The binding energies are lower in the monophosphides than in elemental phosphorus, indicating the presence of anionic phosphorus in these compounds. The trend of increasing phosphorus binding energy through the series from CrP to CoP clearly confirms our expectation of decreasing ionic character in the metal−phosphorus bonding as the electronegativity difference between the elements decreases. Interestingly, theoretical studies on the diatomic gas-phase molecules MP (M = Sc−Cu) also show the same general trend of decreasing ionic character.[26]

Since core-level binding energies are affected by the chemical environment, the charge on the phosphorus atoms in these compounds may be estimated from the P $2p_{3/2}$ binding energies. Binding energies for a large number of compounds containing the same transition metals and phosphorus in a variety of oxidation states (as well as that of elemental phosphorus) are available from the NIST XPS database.[27] If a linear relationship is assumed between the P $2p_{3/2}$ binding energy and the oxidation state, an interpolation of the binding energies for the transition-metal monophosphides suggests P charges of −1.4 in CrP, −1.1 in MnP, −1.0 in FeP, and −0.7 in CoP. A plot of these values versus the electronegativity difference is shown in Figure 4, consistent with the decreasing ionicity of the metal−phosphorus bond through the sequence from CrP to CoP. These values also suggest that the formulation $M^{3+}P^{3-}$ is untenable, and in fact, they are remarkably consistent with the formulation $M^{1+}P^{1-}$ mentioned earlier in which some P−P bonding is implicated. However, caution must be applied because it is difficult to separate the effect of electron count, which modifies the degree of P−P bonding, and the effect of decreased ionicity in the metal−phosphorus bond on the ultimate charge adopted by the phosphorus atoms. Indeed, the trend in P−P bond lengths through the series CrP (2.644 Å) to CoP (2.701 Å),[9] as well as charges calculated in theoretical studies,[13] is opposite to that suggested here, implying that decreased metal-to-phosphorus electron transfer (from CrP to CoP) is the more important effect in determining the binding energies observed.

3.2. Metal $2p_{3/2}$ High-Resolution X-Ray Photoelectron Spectra. Figure 5 shows the high-resolution metal $2p_{3/2}$ spectra for CrP, MnP, FeP, and CoP. The binding energies (Table 1) are similar to those found for the elemental metal (within 0.1−0.2 eV) and to values previously reported by Myers et al.[16] However, the high-resolution spectra presented here show a distinct asymmetric line shape that, to our knowledge, has not been previously interpreted for these compounds. This feature is characteristic of significant metal−metal bonding such as has been proposed for MnP-type structures.[13]

To substantiate the inference of metal−metal bonding, we have collected high-resolution $2p_{3/2}$ spectra for the elemental metals Cr, Mn, Fe, and Co, which are shown in Figure 6. Each spectrum shows an asymmetric line shape skewed to higher binding energy. According to Doniach and Šunjić,[28] this type of line shape arises when valence electrons, interacting with the core hole (produced after photoionization), are excited and scattered from filled states below the Fermi edge to empty conduction states above. Since there is a continuum of states above and below the Fermi edge in a metal, an asymmetric tail comprising many closely spaced states is observed instead of a few distinct satellite peaks.[29] The spectrum for Co metal, however, reveals not only an asymmetric line shape but also a distinct satellite structure (Figure 6d) which has been observed before.[30,31] To properly fit the spectrum, two satellite peaks centered at 5.0 and 3.0 eV away from the main core line were required. Note that the spectrum for CoP also shows two satellite peaks at similar energies as in Co metal, but with much lower intensities (Figure 5d). A detailed interpretation of these satellite peaks is important but is deferred to a later section.

The similarity in the binding energies and line shapes of the metal $2p_{3/2}$ spectra for both the transition-metal mono-

(25) Allred, A. L.; Rochow, E. G. *J. Inorg. Nucl. Chem.* **1958**, *5*, 264−268.
(26) Tong, G. S. M.; Jeung, G. H.; Cheung, A. S.-C. *J. Chem. Phys.* **2003**, *118*, 9224−9232.
(27) Wagner, C. D.; Naumkin, A. V.; Kraut-Vass, A.; Allison, J. W.; Powell, C. J.; Rumble, J. R., Jr. *NIST X-ray Photoelectron Spectroscopy Database*, version 3.4 (web version); National Institute of Standards and Technology: Gaithersburg, MD, 2003 (srdata.nist.gov/xps).
(28) Doniach, S.; Šunjić, M. *J. Phys. C: Solid State Phys.* **1970**, *3*, 285−291.
(29) Hüfner, S. In *Photoemission in Solids II*; Ley, L., Cardona, M., Eds.; Springer-Verlag: Berlin, 1979.
(30) Raaen, S. *Solid State Commun.* **1986**, *60*, 991−993.
(31) Richardson, D.; Hisscott, L. A. *J. Phys. F: Metal Phys.* **1976**, *6*, L127−L134.

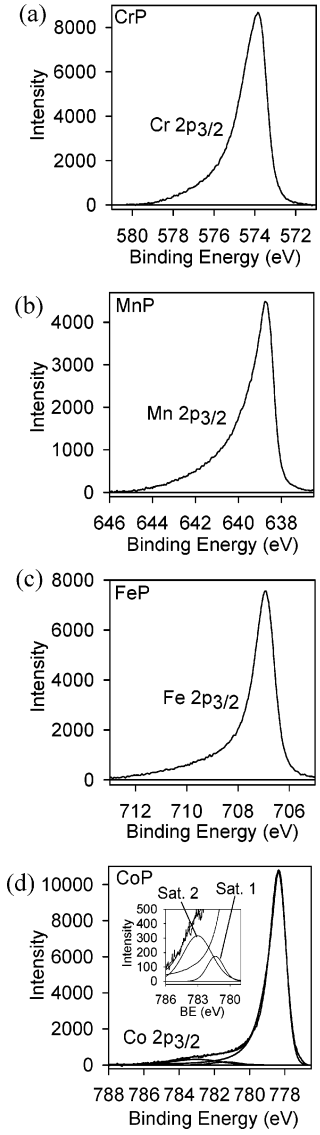

Figure 5. High-resolution metal $2p_{3/2}$ XP spectra for (a) CrP, (b) MnP, (c) FeP, and (d) CoP. The inset in Figure 5d shows the observed low-intensity satellite structure for CoP.

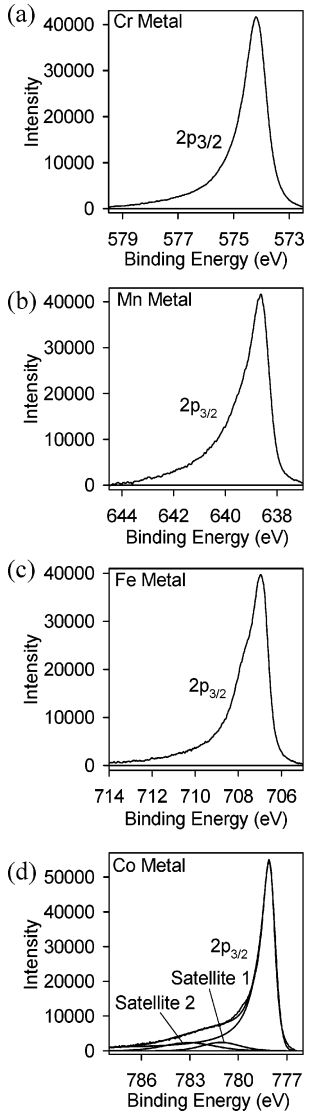

Figure 6. High-resolution $2p_{3/2}$ XP spectra of clean samples of (a) Cr, (b) Mn, (c) Fe, and (d) Co metal.

phosphides and the elemental metals argues for the presence of metal atoms with nearly zero charge and substantial metal−metal bonding in the monophosphides. Relative to a metal atom in a cationic state with a localized electronic structure, photoelectrons from a metal atom participating in extended metal−metal bonding may have a lower binding energy because of the delocalization of electrons in conduction states allowing the atom to experience, on average, greater nuclear screening. As well, the strong hybridization of metal- and phosphorus-based states arising from the primarily covalent nature of the bonding interactions reduces the difference in binding energy of the metal atoms in the monophosphides versus in the elemental metals.[32] In contrast, the difference in binding energy observed for the P atoms in the monophosphides compared to elemental phosphorus suggests that the electrons in the monophosphide P atoms are localized and any bonding within the anionic P substructure is also localized. At first glance, these binding energy results seem to imply a problem with charge neutrality in these transition-metal monophosphides, as the metal atoms are assigned charges of nearly 0 whereas the phosphorus atoms are assigned charges of nearly −1. It is interesting to note that a similar problem was encountered in an earlier band structure calculation, which revealed that the clear presence of some P−P bonding (as evaluated by overlap populations) was not reflected correctly in the charges borne by the phosphorus atoms.[13] Resolving this problem involves a more sophisticated interpretation of the XP spectra, given below.

3.3. Satellite Structure in Co Metal and CoP Co $2p_{3/2}$ Spectra. The satellite structure in the Co $2p_{3/2}$ spectra of Co metal and CoP noted above is also observed in the spectrum of Ni metal, which has received considerable attention in the past.[33−35] Two explanations have been

(32) Anno, H.; Matsubara, K.; Caillat, T.; Fleurial, J.-P. *Phys. Rev. B: Condens. Matter Mater. Phys.* **2000**, *62*, 10737−10743.

(33) Hüfner, S. *Photoelectron Spectroscopy*; Springer-Verlag: Berlin, 1995.
(34) Kemeny, P. C.; Shevchik, N. J. *Solid State Commun.* **1975**, *17*, 255−258.
(35) Hüfner, S.; Wertheim, G. K. *Phys. Lett. A* **1975**, *51*, 299−300.

developed to account for this satellite structure: plasmon loss (loss of kinetic energy of the photoelectron when it interacts with bound valence electrons, causing them to oscillate)[36] and the "two core hole" theory.[33] The former was initially abandoned when no evidence of plasmon loss was found in optical or electron energy loss spectra.[33] Instead, it was suggested that the satellite structure found at 6 eV above the core line in the XP spectrum of Ni metal could arise from final state effects,[33] similar to those proposed by Kotani and Toyozawa.[37] After photoionization, the resulting core hole increases the effective charge operating on the remaining electrons. This increased charge pulls conduction states below the Fermi energy. If the conduction state is empty, then the satellite peak is observed because of a final state containing two holes (one in the core level present after photoionization and one in the valence band). If a filled conduction state is pulled below the Fermi energy, then this final state represents the observed core line.[33] The same description has been applied to describe the satellite peak observed in the spectrum of Co metal.[30]

Although the "two core hole" theory has been widely accepted, there is evidence that the plasmon loss explanation deserves further consideration. Previous electron energy loss studies of the first-row transition metals have revealed the presence of two peaks at <10 eV below the main elastic line for Co and Ni metal.[38,39] These peaks were attributed to plasmon loss, as well as to $M_{4,5}$ ionization.[38] It should be noted that these results were not specifically used to rationalize the nature of the satellite peak found in the XP spectrum of Ni metal during the period in which the "two core hole" theory was developed. Recently, a careful re-examination of REELS data for Ni metal has revealed peaks at a similar energy separation from the main elastic line, as is found for the satellite peak from the core line observed in the Ni $2p_{3/2}$ XP spectrum.[40] These features were attributed to both bulk and surface plasmon structures. Plasmon loss events occurring by interaction of the exiting photoelectrons with valence electrons of atoms located closest to the surface (surface plasmon loss) are lower in energy than those occurring by interaction with valence electrons of atoms located below the surface (bulk plasmon loss).[41] If the presence of the satellite peak in the XP spectrum were really due to the process involved in the "two core hole" theory, then no corresponding transitions should be observed in the REEL spectrum because photoionization does not occur in this experiment.[40] The fact that these features were indeed observed in the REELS data militates against the "two core hole" explanation and instead favors the plasmon loss explanation.

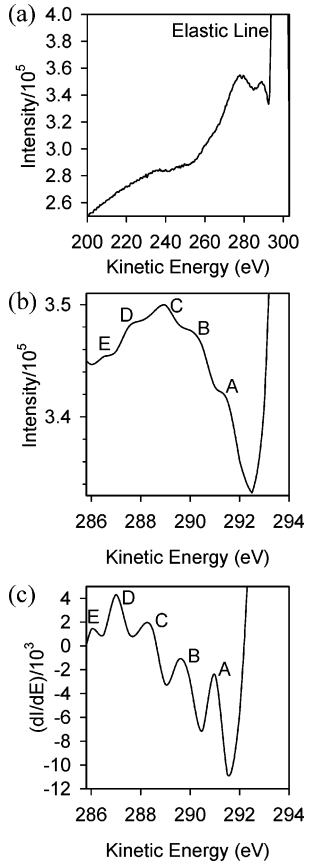

Figure 7. (a) REEL spectrum of Co metal taken at 0.3 keV. (b) Expanded spectrum showing the plasmon loss region located just below the main elastic line. (c) First derivative of the expanded spectrum.

Further, REELS analysis of NiO showed no such similar peaks, as expected since no plasmon loss satellite structures are observed in its corresponding Ni $2p_{3/2}$ XP spectrum.[40] This confirms that the peaks observed for Ni metal are real and not due to noise or other associated spectrometer effects. Plasmon loss peaks normally occur at much higher energy than was observed during this study of Ni metal (typically ~20 eV as determined by EELS).[38,39] However, similar low-energy plasmon loss has been observed by EELS of Mo (110) after deposition of two monolayers of Ba onto the surface.[41] The surface plasmon peak found at 2.6 eV was proposed to arise from interaction of the exiting electrons with the layer of Ba atoms located closest to the surface, whereas the bulk plasmon peak found at 6.7 eV was attributed to interactions of the exiting electrons with the layer of Ba atoms beneath it.[41] These observations imply that the interaction of electrons with atoms found within the uppermost region of a surface results in a much lower energy plasmon loss than is the case deeper within the surface. Moreover, in the initial reports that suggested the presence of lower energy surface plasmon peaks, it was observed that, although these losses were found during experiments using EELS in reflection mode, they were not specifically observed when transmission EELS was used.[39]

To understand the nature of the satellite peaks observed in the XP spectra of Co metal and CoP, a REELS analysis was performed on Co metal (Figure 7). The overall spectrum, taken at 0.3 keV (Figure 7a), compares well with that

(36) Egerton, R. F.; Malac, M. *J. Electron Spectrosc. Relat. Phenom.* **2005**, *143*, 43−50.
(37) Kotani, A.; Toyozawa, T. *J. Phys. Soc. Jpn.* **1974**, *37*, 912−919.
(38) Robins, J. L.; Swan, J. B. *Proc. Phys. Soc., London* **1960**, *76*, 857−869.
(39) Misell, D. L.; Atkins, A. J. *J. Phys. C: Solid State Phys.* **1972**, *5*, 95−106.
(40) Grosvenor, A. P.; Biesinger, M. C.; Zou, F.; Smart, R. St.-C.; McIntyre, N. S. *Surf. Sci.* 2005, submitted.
(41) Gorodetsky, D. A.; Melnik, Yu. P.; Proskurin, D. P.; Sklyar, V. K.; Usenko, V. A.; Yas'ko, A. A. *Surf. Sci.* **1998**, *416*, 255−263.

Table 2. Bulk Plasmon Loss Peak Energies (eV) in Co Metal[a]

line	peak energy	energy separation from elastic peak
elastic peak	295.5	
A	291.5	4.0
B	290.0	5.5
C	289.0	6.5
D	287.5	8.0
E	286.0	9.5

[a] Energies were determined from the first derivative of the REEL spectrum (Figure 7c) taken using a beam energy of 0.3 keV. Surface plasmon loss peaks were also observed in spectra taken at 0.2 keV with energies of 2 and 3 eV from the main elastic line.

obtained by Robins and Swan.[38] In the energy-loss region at ~10 eV below the elastic line, five low-intensity peaks were observed (Figure 7b). The positions of these peaks, which are attributed to plasmon loss, were located more precisely by analyzing a plot of the first derivative of the intensity (Figure 7c) and are listed in Table 2. The peaks labeled A and B are the most intense (after subtraction of the background due to inelastic electron scattering); they are believed to represent bulk plasmon loss and also appear in the corresponding XP spectrum as a broad peak centered at 5 eV above the main $2p_{3/2}$ core line (satellite 2 in Figure 6d). The bulk plasmon event might be represented by two peaks rather than one because of interactions with different valence states, i.e., Co 3d and Co 4s states. Peaks C, D, and E may represent higher-energy plasmon loss or multiple plasmon loss events. The broad satellite peak centered at 3.0 eV above the core line in the XP spectrum of Co (labeled as satellite 1 in Figure 6d) was not observed in the REELS data taken at 0.3 keV, likely because it is overlapped by the intense and broad elastic peak. A REEL spectrum was also taken at a lower beam energy of 0.2 keV (not shown). Intense peaks separated only slightly from the elastic line, at 2 and 3 eV away, were observed and attributed to surface plasmon loss since such peaks were not observed in spectra taken using higher-energy and, thus, less-surface-sensitive electron beams. Thus, it appears that satellite 1 arises from surface plasmon loss and satellite 2 arises from bulk plasmon loss in the XP spectra of Co metal (Figure 6d) and CoP (Figure 5d). As pointed out earlier, these losses most likely arise from interactions of the exiting photoelectrons and valence electrons of atoms located within the uppermost region of the surface. It should also be noted that as the electron beam energy was increased, the higher energy loss peaks were consistently observed, indicating that these are real transitions and not noise.

The Co $2p_{3/2}$ XP spectra of Co metal and CoP could be fitted with individual peaks representing the different plasmon loss structures observed in the REELS data, but it was found to be much simpler to model these loss events using two broad peaks (FWHM > 2 eV). The observation of the plasmon loss peaks in CoP at similar energy separations as those found in Co metal (Table 1) indicates that similar valence electrons are involved in the plasmon loss process (most likely Co 3d and 4s electrons). However, the lower intensity of the satellite peaks in CoP suggests that there are fewer valence electrons around the Co atoms in CoP than in

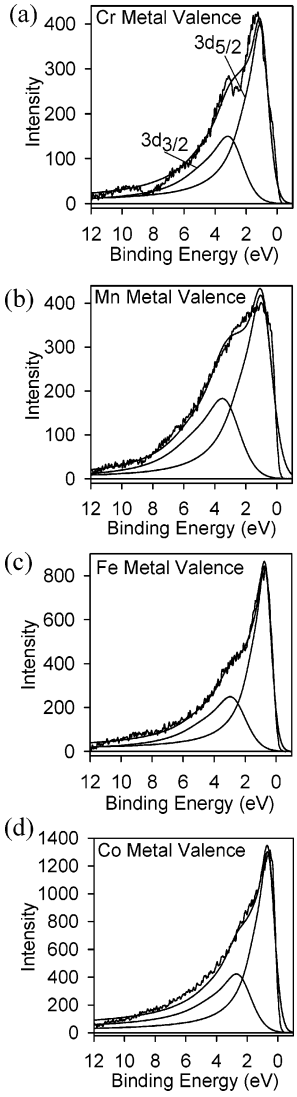

Figure 8. Fitted valence-band spectra of sputter-cleaned samples of (a) Cr, (b) Mn, (c) Fe, and (d) Co metal. The spectra have been fitted using two peaks representing $3d_{5/2}$ and $3d_{3/2}$ states with a fixed intensity ratio of 3:2.

Co metal. That is, analysis of the satellite structure points strongly to the conclusion that, despite their similar binding energies, the Co atoms in CoP are definitely cationic relative to the elemental metal. By analogy, we assert that this argument can be extended to the other monophosphides studied as well.

3.4. Valence-Band Spectra. Comparing the valence-band spectra of the elemental metals and the metal phosphides provides further insight into the bonding interactions present in these compounds. The valence-band spectra of the metals (Figure 8) show a broad peak located at the Fermi edge which can be fitted by two peaks representing $3d_{5/2}$ and $3d_{3/2}$ states with a fixed intensity ratio of 3:2. As was earlier observed in the metal $2p_{3/2}$ spectra (Figure 6), it was important to model these peaks as asymmetric to higher binding energy to properly fit the spectra, indicating that Doniach−Šunjić processes also occur during excitation of the 3d valence electrons.[29] No attempt was made to include a peak representing 4s states since it would be broad and have an energy similar to the 3d states with a lower intensity due to a low

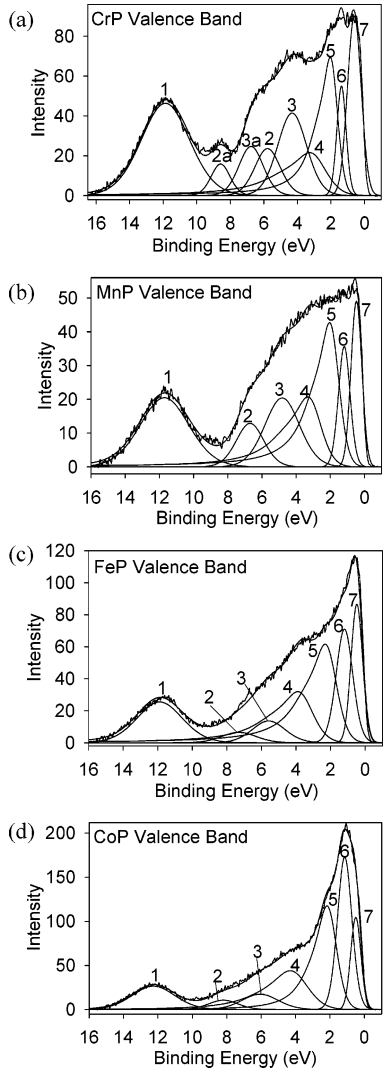

Figure 9. Fitted valence-band spectra of sputter-cleaned samples of (a) CrP, (b) MnP, (c) FeP, and (d) CoP.

electron population.[13,33] In principle, the d orbitals are not quite degenerate and the fit could be improved by employing multiple 3d peak sets, but the two peaks used here were deemed sufficient to give a reasonable fit.

The fitted valence-band spectra of the transition-metal monophosphides are shown in Figure 9. In general terms, the measured valence-band spectra are in excellent qualitative agreement with calculated band structures, which show a sharp Fermi edge and a narrow, metal-based, d band with a high density of states superimposed partially on a broader, largely phosphorus-based p band.[11−13,17,18] They also resemble spectra previously reported for MnP,[4,16,17] FeP,[16,18] and CoSb,[42] but the use of different excitation energies in different studies affects the photoionization cross-sections and thus modifies the peak intensities.[43]

To fit the spectra presented in Figure 9 with both transition-metal and phosphorus states, they were compared to previously reported band structure calculations and XPS results. The region 15−10 eV below E_F has been attributed to P 3s states[15] whereas the broad region above it (8−3 eV) has been attributed to P 3p bonding states.[18] The transition-metal 3d states (containing both t_{2g} and e_g components) have been suggested to lie close to E_F along with P 3p nonbonding states having a similar to slightly lower binding energy.[18] The position of the P 3p nonbonding states lying above the transition-metal 3d states has been implied previously in band structure calculations of transition-metal monophosphides,[18] as well as in the valence-band spectrum of Ni_2P.[44] As an example, the unfitted valence-band spectrum for MnP can be compared to the P 3s, P 3p, and Mn 3d projections of the density of states, as determined from an extended Hückel calculation (Figure 10). The highest BE region can be assigned to P 3s states, the region above it to P 3p states, followed by Mn 3d states; there is also a small contribution of P 3p nonbonding states closest to the Fermi edge. Guided in this manner, we have developed a fitting methodology for the valence spectra of all four compounds, described below.

The superior resolution of the spectra obtained here allows deconvolution into components, labeled from 1 to 7 (Figure 9), in an attempt to separate individual valence states. Although there is some degree of overlap, each of the peaks shown is required to optimize the fit to the spectrum, especially the shoulder features, which appear reproducibly. Consistent with calculated band structures and previously reported XPS results, the following assignments are proposed. Peak 1 represents P 3s states, and peaks 2 and 3 represent P $3p_{1/2}$ and $3p_{3/2}$ states, respectively, with a fixed intensity ratio of 1:2. Peaks 4 and 5 represent the t_{2g} set of the metal 3d states and were fitted with an asymmetric line shape profile (as was observed in the valence-band spectra of the elemental metals, discussed above) with a fixed intensity ratio of 3:2 ($3d_{5/2}/3d_{3/2}$). Peak 6 represents the e_g set (M−P antibonding) of the metal 3d states and was fitted with a single profile constrained to represent spin-up electrons. Peak 7 likely represents essentially nonbonding P 3p states. To properly fit this state, only a Gaussian line shape was required, suggesting that spectrometer effects are dominant; lifetime effects are probably small, given the low energy of this feature, which appears just below the Fermi edge. The identity of peaks 2a and 3a found in the spectrum of CrP is discussed below. The binding energies and FWHM values of the component peaks used to fit the valence-band spectra are listed in Table 3 and were optimized to provide the best fit.

Consistent with the expectation that the major orbital interactions should be between the metal 3d and phosphorus 3p states, these peaks show considerable overlap in energy. In this analysis, we have made a distinction for the phosphorus 3p states, which are dispersed over a very wide energy range according to band structure calculations (Figure 10c), into those that are clearly bonding in character (near 5−7 eV) and those that are essentially nonbonding in character (close to the Fermi edge). Justifying this analysis, we note that the P 3p bonding peaks are wide and their

(42) Liang, K. S.; Chen, T. *Solid State Commun.* **1977**, *23*, 975−978.
(43) Scofield, J. H. *J. Electron Spectrosc. Relat. Phenom.* **1976**, *8*, 129−137.
(44) Kanama, D.; Oyama, S. T.; Otani, S.; Cox, D. F. *Surf. Sci.* **2004**, *532*, 8−16.

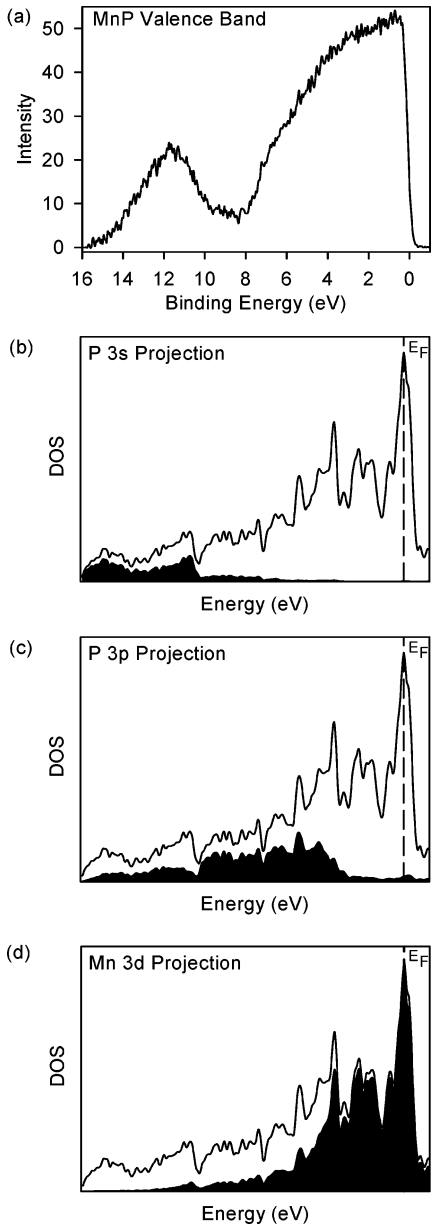

Figure 10. (a) Valence-band spectrum of MnP compared to the calculated projections of the density of states for (b) P 3s, (c) P 3p, and (d) Mn 3d orbitals. The shaded regions represent the projections, whereas the solid line represents the total density of states. The dashed line marks the Fermi level.

binding energies show a significant shift through the series CrP to CoP (Table 3), which is to be expected if they are truly involved in bonding interactions. In contrast, the P 3p nonbonding peaks are narrow and their binding energies show little change. Interestingly, the binding energies of the P 3s states (near 12 eV) show only a slight shift on going from CrP to CoP, similar to that observed for the obviously nonbonding P 2p states, implying that they are less important than the 3p states in bonding interactions as has been suggested previously.[15] The metal 3d states, split into t_{2g} and e_g components, have similar energies as those in the valence-band spectra of the pure metals. This verifies our earlier conclusion derived from analysis of the satellite structure in the metal $2p_{3/2}$ core spectra of Co metal and CoP which showed that during the plasmon loss process in which the

Table 3. Binding Energies (eV) of Component Peaks in Valence-Band Spectra of MP (M = Cr, Mn, Fe, Co)[a]

peak	assignment	CrP	MnP	FeP	CoP
1	P 3s	11.8 (3.4)	11.7 (3.4)	11.9 (3.1)	12.3 (2.9)
2	P $3p_{1/2}$	8.6 (1.3),[b] 5.8 (1.8)	6.7 (1.9)	7.3 (2.4)	8.2 (2.0)
3	P $3p_{3/2}$	6.8 (1.7),[b] 4.3 (2.0)	4.8 (2.4)	5.6 (2.2)	6.1 (2.5)
4	M $3d_{3/2}$ t_{2g}	3.2 (2.2)	3.3 (1.8)	3.9 (2.0)	4.3 (2.3)
5	M $3d_{5/2}$ t_{2g}	2.0 (1.0)	2.0 (1.3)	2.3 (1.5)	2.2 (1.3)
6	M $3d_{5/2}$ e_g	1.4 (0.7)	1.2 (0.8)	1.2 (1.1)	1.1 (1.0)
7	P 3p	0.6 (1.0)	0.5 (0.8)	0.5 (0.8)	0.5 (0.7)

[a] FWHM values (eV) are indicated in parentheses. [b] A second set of higher-binding-energy P $3p_{1/2}$ and P $3p_{3/2}$ peaks, labeled, respectively, as peaks 2a and 3a in Figure 9a, is present in the spectrum of CrP.

exiting photoelectrons interacted with the valence electrons of the metal atoms in the pure metal and in the monophosphide, the photoelectrons lost similar amounts of energy. The general increase in the binding energies of the metal $3d_{3/2}$ t_{2g} peak with a concomitant increase in the energy separation between this peak and the corresponding $3d_{5/2}$ t_{2g} peak as the atomic number of the metal increases is normally observed in XP spectra.[24]

The electron populations of the different orbital states in the valence-band spectra were extracted from normalized peak intensities, C_i, according to eq 1.[45]

$$C_i = \frac{I_i/(\sigma_i\lambda_i)}{\sum_{j=1}^{n} I_j/(\sigma_j\lambda_j)} \qquad (1)$$

In this equation, $I_i/(\sigma_i\lambda_i)$ represents the corrected intensity of the peak under consideration and $\sum_{j=1}^{n} I_j/(\sigma_j\lambda_j)$ represents the sum of the corrected intensities from all of the peaks present in the valence-band spectrum. The values of the photoionization cross-section (σ) and inelastic mean free path (IMFP, λ) corrections are listed in Table 4. Much of the variation in the shapes of the valence-band spectra shown in Figure 9 arises from the different cross-sections for the metal 3d states. The number of electrons in each state was then calculated assuming a total of 11, 12, 13, and 14 electrons in the valence band of CrP, MnP, FeP, and CoP, respectively. The results of these calculations are summarized in Table 5.

From the total electron populations, a charge of about +0.7 for the metal and about −0.7 for the phosphorus atoms in each of these compounds was deduced, providing further support for the approximate formulation $M^{1+}P^{1-}$ described earlier. The electron populations of individual states also correlate with some of the general trends seen in the crystal structures. The population of the metal t_{2g} states, which are involved in metal−metal bonding, increases through the series CrP (4.2 e^-) to CoP (5.2 e^-), consistent with the

(45) Watts, J. F.; Wolstenholme, J. *An Introduction to Surface Analysis by XPS and AES*; Wiley: Rexdale, 2003.
(46) Brillson, L. J.; Ceasar, G. P. *Surf. Sci.* **1976**, *58*, 457−468.
(47) Tougaard, S. *QUASES-IMFP-TPP2M: Database for Calculation of IMFPs by TPP2M Formula*, version 2.1; QUASES-Tougaard, Inc.: Odense, Denmark, 2000 (www.quases.com).

Table 4. Corrections Applied to Intensities of Peaks in Valence-Band Spectra of MP (M = Cr, Mn, Fe, Co)[a]

atom	state	photoionization cross-section, σ	IMFP, λ (Å)
Cr	$3d_{3/2}$	0.0264	26.2
	$3d_{5/2}$	0.0387	
Mn	$3d_{3/2}$	0.0424	25.9
	$3d_{5/2}$	0.0622	
Fe	$3d_{3/2}$	0.0694	25.9
	$3d_{5/2}$	0.1017	
Co	$3d_{3/2}$	0.1082	24.0
	$3d_{5/2}$	0.1582	
P	3s	0.1116	33.9
	$3p_{1/2}$	0.0354	
	$3p_{3/2}$	0.0708	

[a] The P $3p_{1/2}$ and $3p_{3/2}$ cross-sections were corrected on the basis of comparison of experimental cross-sections determined by Brillson and Ceasar[46] to those calculated by Scofield.[43] All other cross-sections listed are those calculated by Scofield.[43] These cross-sections were determined for an excitation energy equal to that of Al Kα X-rays.[43] The IMFP values were determined using the QUASES IMFP calculator.[47]

Table 5. Electron Populations in MP (M = Cr, Mn, Fe, Co)

state	CrP	MnP	FeP	CoP
P 3s nonbonding	1.3	1.4	1.6	1.4
P 3p bonding	3.3[a]	3.1	1.9	2.4
M 3d t_{2g}	4.2	5.0	5.2	5.2
M 3d e_g antibonding	1.1	1.4	2.3	3.0
P 3p nonbonding	1.1	1.1	2.1	2.0
total P	5.7	5.7	5.6	5.8
total M	5.3	6.3	7.4	8.2
total number of e^-	11.0	12.0	13.0	14.0

[a] 1.1 e^- in P−P bonding states (peaks 2a and 3a in Figure 9a) and 2.2 e^- in Cr−P bonding states (peaks 2 and 3 in Figure 9a).

shortening of the average metal−metal bond lengths (2.782−2.678 Å),[9] if contacts less than 3.0 Å are considered significant. The population of the phosphorus 3p bonding states, which are involved in both metal−P and possibly P−P bonding, decreases on going from CrP (3.3 e^-) to CoP (2.4 e^-), consistent with the lengthening of P−P bond lengths (2.644−2.701 Å).[9] Given that these are weak interactions at best, any manifestation of P−P bonding states should be most prominent in CrP. Indeed, the valence-band spectrum of CrP (Figure 9a) reveals extra shoulders that can be fit by invoking a second set of higher-binding-energy P 3p states (peaks 2a and 3a in Figure 9a) which result from P−P bonding, in addition to the first set of P 3p states (peaks 2 and 3 in Figure 9a) at lower binding energy which are due to Cr−P bonding. Table 5 shows that the electron population in the P−P bonding states is only half as large as in the Cr−P bonding states. On progressing to the other transition-metal monophosphides of the series, a trend toward populating the nonbonding P 3p states, at the expense of the bonding P 3p states, is observed which is consistent with the gradual disappearance of the already weak P−P bonds. In the case of FeP and CoP, the values of the electron populations of the phosphorus-based states suggest that there is negligible, if any, P−P bonding. Size effects cannot be ruled out as being responsible for these trends in both metal−metal and phosphorus−phosphorus bonding behavior. Progressing along the first-row transition-metal series, we see a contraction of the structure, which may serve as the true driving force for the observed trends. The occurrence of ferromagnetism in some of these compounds also complicates the interpretation of the electronic structure.

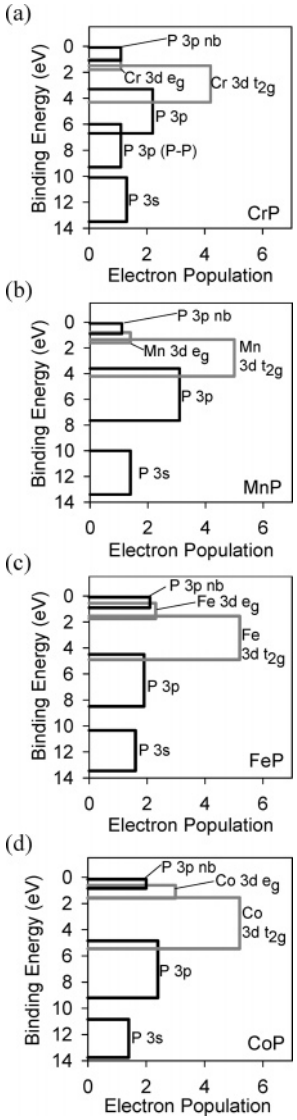

Figure 11. Energy-level diagrams for (a) CrP, (b) MnP, (c) FeP, and (d) CoP.

From the above analysis of the electron populations deduced from the valence-band spectra, experimental energy-level diagrams for these four monophosphides can be constructed. Figure 11 presents plots of the electron population versus energy. These diagrams are consistent with theoretical band structure calculations. Band dispersion and electron populations of different metal- and phosphorus-based states agree well with partial density of states curves and the bonding, nonbonding, or antibonding character of states agrees well with crystal orbital overlap population curves.[13]

4. Conclusion

Core and valence-band X-ray photoelectron spectra have been obtained for the series of isostructural MnP-type transition-metal monophosphides CrP, MnP, FeP, and CoP. The high-resolution phosphorus 2p spectra indicated that the charge of the P atoms is close to −1, as determined from their binding energies. The increase in the phosphorus 2p

binding energies through the sequence CrP to CoP confirms the decrease in ionicity of the metal-phosphorus bond as the difference in electronegativity between the atoms diminishes.

The high-resolution metal $2p_{3/2}$ spectra of the monophosphides closely resemble those of the parent transition metals in terms of both binding energy and line shape. The metal atoms in the monophosphides possess a delocalized electronic structure arising from the presence of extended metal−metal bonding, which provides greater nuclear shielding than for isolated atoms. The satellite structure observed in the Co $2p_{3/2}$ spectra of both Co metal and CoP was confirmed by REELS analysis of Co metal. This feature arises from plasmon loss and not as the result of a "two core hole" final state effect. The common satellite structure for both Co metal and CoP implies that the valence electrons of the metal atoms have similar energies, as was also confirmed by analysis of the valence-band spectra. However, there are fewer valence electrons around the metal atoms in CoP than in Co metal, implying a cationic state which is consistent with the anionic state of the phosphorus atoms.

The valence-band spectra agree well with calculated band structures. We demonstrate a useful approach for analyzing the valence-band spectra by fitting these bands with component peaks representing electronic states and their populations. The major orbital interactions arise between the metal 3d and phosphorus 3p states. The electron count for the metal and phosphorus atoms, extracted from the corrected intensities of these component peaks, favors the formulation $M^{1+}P^{1-}$ in which both metal−metal and phosphorus−phosphorus bonding are present. The metal−metal bonding network involves highly delocalized states, similar in character to those of the pure metal, whereas the phosphorus−phosphorus bonding network, which is already weak for CrP and MnP and probably negligible for FeP and CoP, involves localized covalent bonding. Energy-level diagrams were constructed from the valence-band spectra and extracted electron populations, which compare well to calculated band structures. This type of bonding analysis derived from analysis of experimental photoelectron spectra is complementary to theoretical calculations and may be generalized to study the bonding interactions involved in other inorganic solids.

Acknowledgment. The Natural Sciences and Engineering Research Council (NSERC) of Canada supported this work through Discovery Grants to R.G.C. and A.M.. We thank Dr. Murray Gray (Director) for providing access to the Kratos XPS and Dr. Dimitre Karpuzov (Facility Manager) for assistance with instrumentation at the Alberta Centre for Surface Engineering and Science (ACSES) at the University of Alberta. ACSES is operated through capital funding from the Canada Foundation for Innovation (CFI), which provides interim operating support, and Alberta Innovation and Science. We thank Dr. S. Ramamurthy (Surface Science Western, University of Western Ontario) for performing the REELS analysis of Co metal, as well as Ms. Christina Barker (Department of Chemical and Materials Engineering, University of Alberta) for assistance with the SEM-EDX analysis. A.P.G. thanks the University of Alberta for support.

IC051004D